



Assessment of Aquifer Indices in Kano State, Nigeria Using Aeromagnetic and Digital Elevation Model Data



Samir Auwalu^{1*}, Muhammad Saleh^{2}, Maitama A. Yusuf Hotoro^{3}, Hamza Salihu Adamu^{4}

¹ Department of Physics, Aliko Dangote University of Science and Technology, 713101 Wudil, Nigeria

² Department of Physics, Bayero University, 700241 Kano, Nigeria

³ Electricity and Fossil Fuels Department, Energy Commission of Nigeria, P.M.B. 358 Abuja, Nigeria

* Correspondence: Samir Auwalu (samirdudugk@students.kustwudil.edu.ng)

Received: 07-22-2024

Revised: 08-25-2024

Accepted: 08-30-2024

Citation: S. Auwalu, M. Saleh, M. A. Y. Hotoro, and H. S. Adamu, "Assessment of aquifer indices in Kano State, Nigeria using aeromagnetic and digital elevation model data," *Acadlore Trans. Geosci.*, vol. 3, no. 3, pp. 135–150, 2024. <https://doi.org/10.56578/atg030302>.



© 2024 by the author(s). Published by Acadlore Publishing Services Limited, Hong Kong. This article is available for free download and can be reused and cited, provided that the original published version is credited, under the CC BY 4.0 license.

Abstract: Aeromagnetic and Digital Elevation Model (DEM) data were analyzed to identify subsurface water-bearing zones and examine the topographical trends of surface and basement complex rocks in a portion of Kano State, Nigeria, bounded by latitudes 8°00'00"N to 9°00'00"N and longitudes 11°30'00"E to 12°30'00"E. The aeromagnetic data, sourced from the Nigerian Geological Survey Agency (NGSA), were subjected to filters, including Residual Magnetic Intensity (RMI) and Source Parameter Imaging (SPI), to estimate residual magnetic fields and depths to the basement complex rocks. The SPI results revealed two distinct depth classes: deeper and shallow regions. Deeper zones, characterized by depths ranging from 123.1 m to 414.4 m, were identified in the following areas: between 8°00'00"N and 8°38'24"N, 12°12'00"E to 12°30'00"E; 8°49'48"N to 9°00'00"N, 12°12'00"E to 12°30'00"E; 8°00'00"N to 8°07'12"N, 11°40'48"E to 12°00'00"E; 8°21'36"N to 8°37'48"N, 11°40'48"E to 12°00'00"E; 8°51'03"N to 9°00'00"N, 11°40'48"E to 12°00'00"E; and 8°14'24"N to 8°22'12"N, 11°33'36"E to 11°38'24"E. These regions, characterized by depression-like features, were suggested as optimal zones for groundwater exploration. The topographical analysis of the surface indicates that rainwater and leachates were transported toward the northern region of the study area, which exhibits relatively low elevations (448 m to 468 m above mean sea level). This region was identified as a likely accumulation area for surface water. The fresh basement complex rocks were observed to gently slope from south to north, with depth values ranging from 112.6 m to 117.7 m in deeper areas and 91.6 m to 109.8 m in shallower zones. The flow direction of surface water aligns with the underlying basement rock structure, suggesting that surface water runoff is likely influencing aquifer recharge processes. A cross-correlation coefficient of -0.99981 was observed between the surface and basement complex rock trends, indicating a strong inverse relationship between the two topographies. Consequently, the surface water accumulation zone was inferred to be a critical aquifer recharge area, though it may also facilitate the leaching of contaminants into the groundwater system, raising potential concerns for aquifer quality.

Keywords: Topography; Aeromagnetic; Groundwater; Aquifer; Basement complex rock; Digital elevation model

1 Introduction

Geophysical techniques are frequently applied to map and investigate basement topography and groundwater potential areas in both basement and sedimentary formations. Researchers in different parts of the world have conducted studies in groundwater investigation using various geophysical methods such as electrical resistivity, gravity, radiometric, seismic, etc. The methods were not limited to groundwater investigation but useful in the fields of archeology, engineering, and environmental studies.

In recent years, the need for large-area coverage has given rise to aerial and remote-sensing methods such as aeromagnetic, aeroradiometric, aerogravity and remote sensing. The most used methods are the aeromagnetic and remote sensed methods because of cost effectiveness, data availability and large-area coverage. The application of aeromagnetic and remote sensed data [1–7] indicates the robustness of the aeromagnetic method, though there is a need for other methods for supplementation. Therefore, most researchers have integrated two or more geophysical methods and remote sensing data for optimal results [8, 9].

Groundwater investigation is one of the most recent areas that has aroused the interest of geoscientists. This ranges from locating groundwater potential areas, groundwater contamination, to aquifer recharge sources. Hussein et al. [10] used remote sensing and aeromagnetic data in their integrated approach based on groundwater mapping around Sohag in upper Egypt and concluded that the integrated approach offer a powerful and effective tool to assist in developing a plan to manage groundwater in arid areas. The colorless, odorless and tasteless nature of water is not a litmus test of its purity. Therefore, the quality of groundwater is affected by factors such as geology, climate, waste water drainages and anthropogenic activities [11]. Other factors includes aquifer depth, net recharge, and topography [12]. Most researchers are more concerned with the contamination location proximate to dwelling areas without minding the leachate flow to other areas due to rainwater. The surface flow of this leachate could accumulate in rivers, lakes, drainages and ponds, which saves sources of aquifer recharge, leading to groundwater contamination. However, identifying the surface water flow pattern, basement topography and aquifer network could help mitigate groundwater contamination.

In this study, aeromagnetic and DEM data were used to assess and map out the potential aquifers, aquifer recharge sources and vulnerable areas of potential groundwater contamination sources in the study area.

The magnetic method theory is categorized into data acquisition and data interpretation theories. The total magnetic field intensity (T) at a region [13] is given as:

$$T = \mu_0 H(1 + k) \quad (1)$$

where, H is the magnetic strength, k is the magnetic susceptibility, and μ_0 is the permeability. T is subjected to polynomial fitting using the polynomial $P(x, y)$ equation [14] as:

$$P(x, y) = a + bx + cy \quad (2)$$

where, a , b , and c are constants obtained from the fitting; and x and y are the geographic coordinates of points under consideration. In this analysis, $P(x, y)$ is taken as the regional magnetic intensity (R) that is removed from T to obtain the residual magnetic intensity (RMI):

$$RMI = T - R \quad (3)$$

Developed by Telford et al. [14], the source parameter imaging (SPI) method is used to calculate depth for fresh basement complex rocks [15]. The depth (D) [14] is expressed as:

$$D = \frac{1}{\sqrt{\frac{\partial^2 T}{\partial x^2} + \frac{\partial^2 T}{\partial y^2}}} \quad (4)$$

The tilt angle [14] is given by:

$$\theta = \arctan \left(\frac{\frac{\partial T}{\partial z}}{\sqrt{\frac{\partial^2 T}{\partial x^2} + \frac{\partial^2 T}{\partial y^2}}} \right) \quad (5)$$

2 Study Area

The study area is located around Danbatta, Harbau, Makoda, Maraki, Kore, Bagwai, Tsanyawa, Gurjiya, Tofa, Kiru, Kumbotso, Dawakin Kudu, Dawakin Tofa, Rano, Kibiya and Kafin Chiri which lies within the latitudes 11°30'0"N to 12°30'0"N and longitudes 8°00'0"E to 9°00'0"E, as shown in Figure 1, and the size of the study area is approximately 17330 km².

The study area is located within the Nigerian basement complex, which forms part of the Pan African mobile belt and lies between the West African Craton and the Tuareg Shield. Earlier research has linked the overall emplacement of the Nigerian basement complex to the earliest orogenic events that affected the African continent. The basement complex rocks include gneisses, migmatites, and meta-sediments of Precambrian ages that have been intruded by a series of Pan African age rocks, as shown in Figure 2. These rocks have undergone varying degrees of metamorphism and granite intrusions through tectonometamorphic cycles, converting them largely into migmatites and granite-gneiss [16, 17].

Younger meta-sediments, believed to be of Upper Proterozoic age, are thought to have been deposited on the granitised basement and were subsequently folded during the Pan-African Orogeny. They are low-grade metamorphic rocks, and are now represented as synclinal troughs among older rocks in northwestern Nigeria. Intrusive basement rocks and the younger supracrustal cover are series of intermediate and acid plutonic rocks, known as the older granite suites. These are charnockites, diorites, fayalites, quartz-monzonites (Bauchites) and gabbroic earlier rocks. Migmatisation has differently affected all the earlier rocks as well as the large-scale conversion of basement gneisses and migmatites [18].

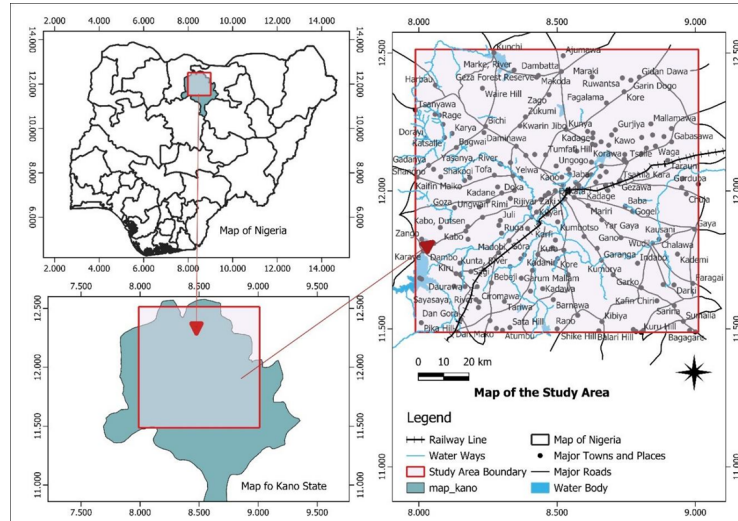


Figure 1. Map of the study area

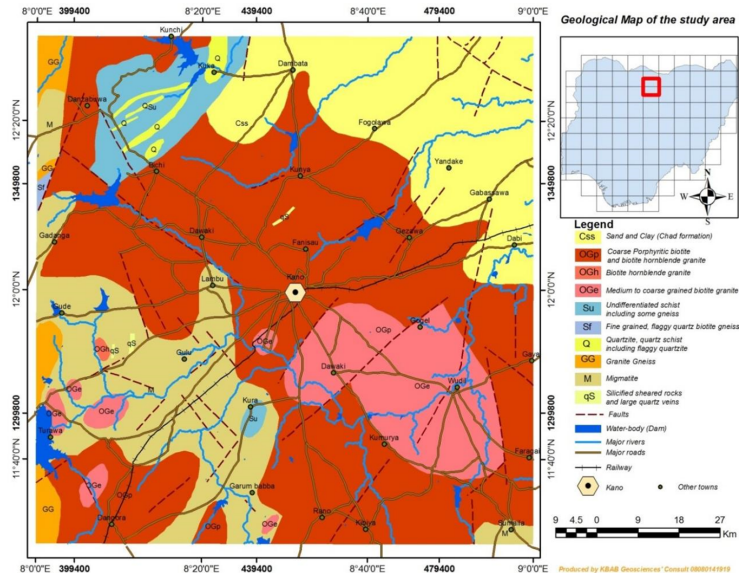


Figure 2. Geological map of the study area

The study area's hydro-geologic aquifer units are divided into two categories: unconsolidated Chad formation sediments and crystalline basement units. In the basement rocks, groundwater is located in underlying fracture zones or in areas where the rocks have weathered considerably. In contrast, sands and gravels contain groundwater in the Chad formation. The study area's groundwater typically lies in the upper few meters of the weathered and fractured basement, and the aquifer system's thickness ranges from 10 to 45 m [19, 20].

Where the pores and fractures are connected (permeable rocks), groundwater can freely flow and is typically stored within the pore spaces and fractures in rocks. Thus, there is a greater chance of groundwater accumulation in porous or fractured rocks. Another factor influencing groundwater availability is the amount and intensity of rainfall. The hydrogeology of the study area was classified into four primary geological provinces: Precambrian basement rocks, volcanic rocks, unconsolidated sediments, and consolidated sedimentary rocks. Groundwater is typically

found in the upper few meters of weathered rocks in basement rocks and in extremely permeable areas between lava flows in volcanic rocks. Consolidated sediments contain groundwater in the weathered zones and pore spaces of sandstones or fractures in limestone [21].

The interconnected aquifers that have been found at (i) soft overburden aquifers, (ii) partially weathered/fractured basement aquifers, and (iii) volcanic rock aquifers in the younger granite areas make up Kano State's crystalline hydrogeological unit. The soils, clays, colluviums, and saprolite make up the soft overburden aquifer. The fractured basement aquifer is composed of slightly weathered and fractured gneissic rocks and fractured and jointed granites. Only in areas where metamorphic and igneous rocks are fractured are volcanic rock aquifers permeable, and they typically only produce a small amount of groundwater. Because of the limited depth of the regolith, its clay content, and the localized occurrences of fractures and joints, the groundwater in the basement rocks is low, and borehole success rates are lower [19].

The sandy belt that makes up Kano State's sedimentary hydrogeologic region is ideal for the placement of hand-dug wells and boreholes. It is made up of the aquifers of the Chad formation and an alluvial deposit aquifer, which is located in river channels and is made up of sandy clays and sands that are typically less than 5 m thick. This kind of aquifer is primarily found in hand-dug wells. The biggest groundwater potential has been found in the restricted regions of the sedimentary formations, which include confined and semi-confined aquifers as well as perched aquifers [19].

The climate of the study area is the same as that of Kano State which is comprised of two climate conditions: tropical wet and dry type. The rainy season occurs between June and September, while the dry season is marked by variable temperatures. During the hot weather, temperatures range from 39°C to 45°C, with lower temperatures during the Harmattan period [17]. The vegetation of the area is Sudan savannah with scattered trees and short grasses. The mean annual rainfall in the area ranges from 1000 mm to 635 mm [22].

3 Methodology

Intangible materials, including aeromagnetic data, DEM data, Oasis Montaj 8.4, Surfer Version 25.0, ArcGIS 10.8 and Microsoft Excel, were used to isolate areas with high groundwater potential and groundwater contamination.

3.1 Aeromagnetic Data

Aeromagnetic datasheets of sheet 57 (Kunya), sheet 58 (Bichi), sheet 80 (Kabo) and sheet 81 (Wudil) were acquired from NGSA. A high-resolution airborne geophysical survey involving magnetic survey was carried out by NGSA with the help of the Furgo Airborne Survey Limited, Johannesburg, from 2004 to 2009, covering the entire country with the aim of developing a geologic map of the mineral resources of the country. Details of the survey equipment and flight specifications are given in Table 1.

Table 1. Survey equipment and flight parameters

Data Sensors on Board	Airborne Magnetic Gradient and GR320-3 (NaI) Multichannel Radiometric Gamma-ray Spectrometer
Data sensors on board	Airborne magnetic gradient and GR320-3 (NaI) multichannel radiometric gamma-ray spectrometer
Flight line spacing	500 m
Terrain clearance	80 m
Flight direction	NW-SE
Tie line spacing	2000 m
Tie line direction	NE-SW

Total Magnetic Intensity (TMI) data obtained were prepared and gridded using the minimum curvature gridding method in Oasis Montaj 8.4. The TMI grid obtained was transferred into ArcGIS environment for further processing and the TMI map of the study area was obtained, as shown in Figure 3.

The TMI data obtained were subjected to regional-residual separation using polynomial fitting, as shown in Eqs. (2) and (3). The regional and residual data obtained were gridded and transferred to the ArcGIS environment to produce the regional and residual maps of the study area, as shown in Figures 4 and 5.

The SPI depth to the basement rock was calculated from the RMI data using polynomial fitting, as shown in Eq. (4). The SPI data obtained were gridded in the Oasis Montaj environment using the minimum curvature gridding method. The grid obtained was transferred to the ArcGIS environment and the SPI map of the area was developed, as shown in Figure 6. On the SPI map, deeper regions were isolated using polygons marked X, Y, Z, K, M, and N and the coordinates of the polygons were recorded, as shown in Table 2.

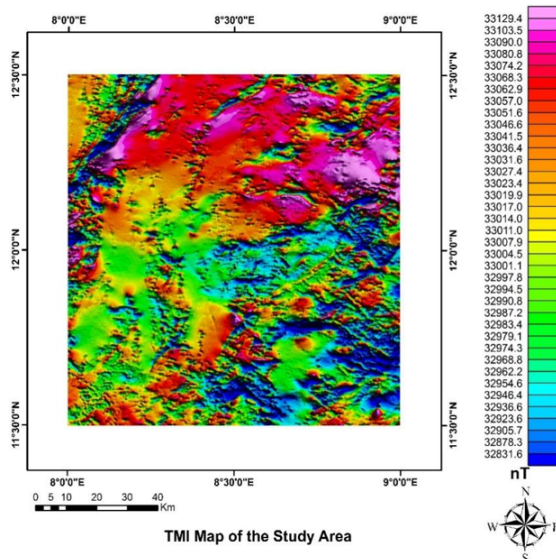


Figure 3. TMI map of the study area

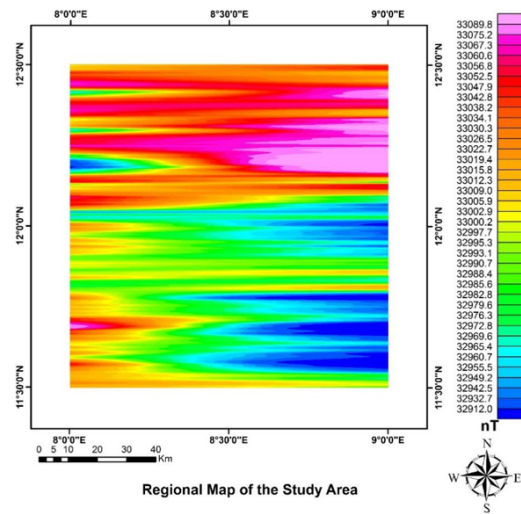


Figure 4. Regional map of the study area

Table 2. Locations of possible aquifers

Polygon	Latitude (N)	Longitude (E)	Depth (m)
X	8°00'00" – 8°38'24"	12°12'00" – 12°30'00"	111.8 - 575.0
Y	8°49'48" – 9°00'00"	12°12'00" – 12°30'00"	139.0 - 447.5
Z	8°00'00" – 8°07'12"	11°40'48" – 12°30'00"	160.2 - 484.5
K	8°21'36" – 8°37'48"	11°40'48" – 12°00'00"	173.0 - 539.9
M	8°51'36" – 9°00'00"	11°40'48" – 12°00'00"	141.7 - 385.6
N	8°54'00" – 8°22'12"	11°33'36" – 11°38'24"	150.8 - 512.6

The SPI data were further subjected to residualization using polynomial fitting, as shown in Eqs. (2) and (3). The regional depth data obtained from residualization were gridded and the regional depth grid was obtained. The regional depth grid was transferred to the ArcGIS environment where the topographic map of the regional fresh basement complex rock depth was produced, as shown in Figure 7. The regional SPI depth data were gridded in Surfer using the minimum curvature gridding technique and cross-sections were obtained from the fresh basement complex rock grid by drawing lines A-A' and B-B' perpendicular to the study area and lines C-C', D-D', E-E', F-F' and G-G' diagonal to the study area, as shown in Figure 8. The corresponding seven profiles obtained from the cross-sections are shown in Figures 9-15.

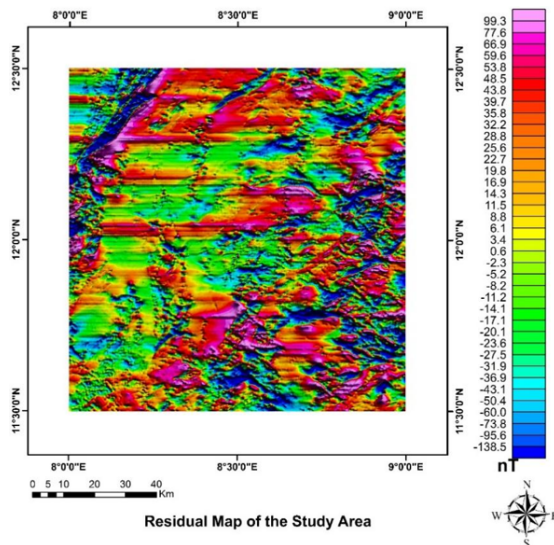


Figure 5. Residual map of the study area

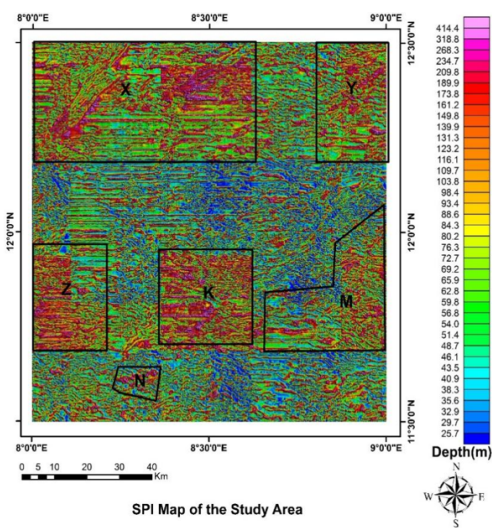


Figure 6. SPI map of the study area

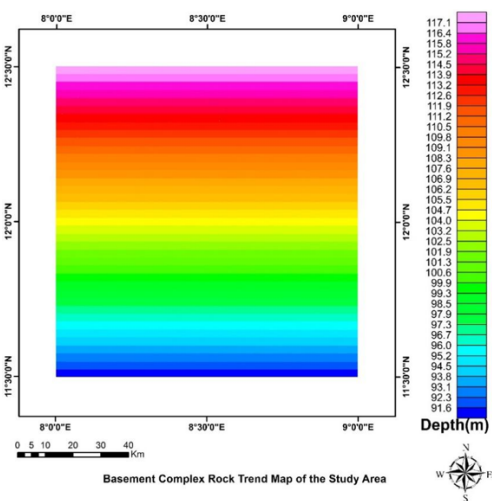


Figure 7. Regional trend of fresh basement complex rocks in the study area

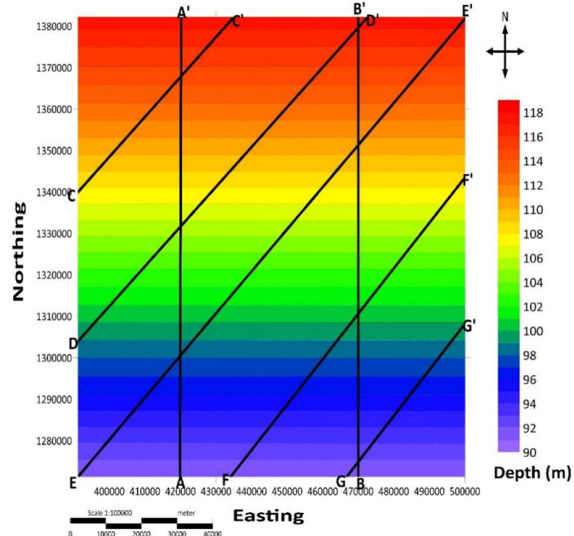


Figure 8. Topography map of fresh basement complex rocks showing profile lines

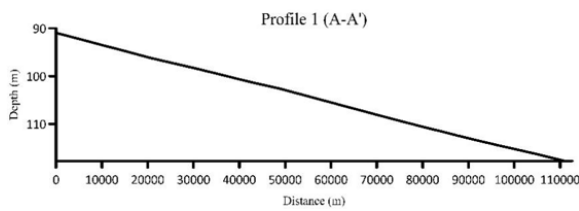


Figure 9. Profile 1 showing the cross-section A-A'

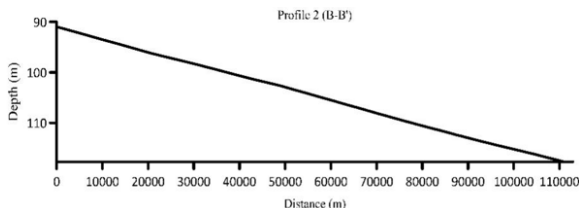


Figure 10. Profile 2 showing the cross-section B-B'

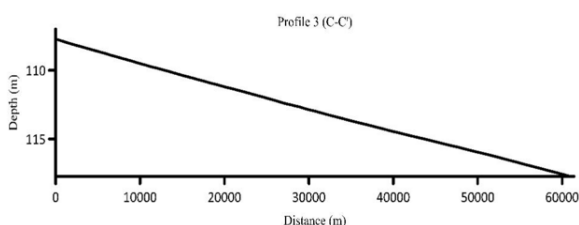


Figure 11. Profile 3 showing the cross-section C-C'

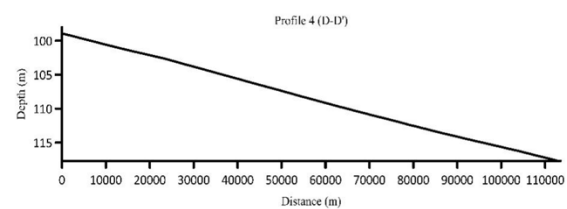


Figure 12. Profile 4 showing the cross-section D-D'

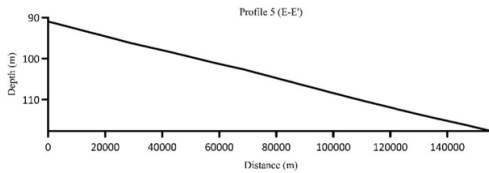


Figure 13. Profile 5 showing the cross-section E-E'

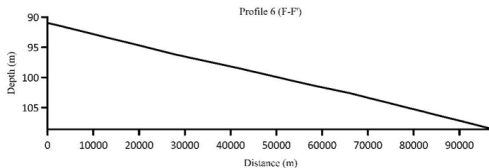


Figure 14. Profile 6 showing the cross-section F-F'

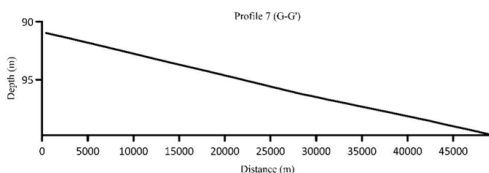


Figure 15. Profile 7 showing the cross-section G-G'

3.2 DEM

The DEM taken at 30 m above the mean sea level of Kano State was downloaded from hppts:dwtkns.com/srtm30m/ on 11/06/2024. The Shuttle Radar Topographic Mission (SRTM)-DEM data were transferred to the ArcGIS environment and the area of interest was windowed out using the study area boundary polygon from the DEM data. The 30 m DEM data were used to calculate the topographic model parameter and used for the geomorphological analysis.

The DEM data were extracted from the SRTM-DEM data of Nigeria. The data obtained were gridded using the minimum curvature gridding method and were further processed in an ArcGIS environment and Surfer version 25.0. The DEM map of the study area was obtained, as shown in Figure 16.

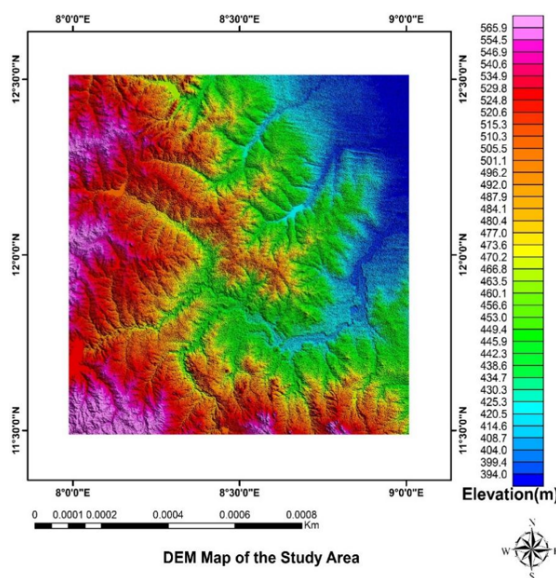


Figure 16. DEM map of the study area

The DEM grid data of the study area were subjected to residualization and the regional and residual grid data were obtained. The regional grid data were gridded and contoured in Oasis Montaj and Surfer. The grids obtained were transferred to the ArcGIS environment to obtain the regional surface topographic map of the area, as shown

in Figure 17. The grid was also transferred to Surfer and cross-section lines were drawn, as shown in Figure 18. Profiles obtained from the cross-section lines are shown in Figures 19-25.

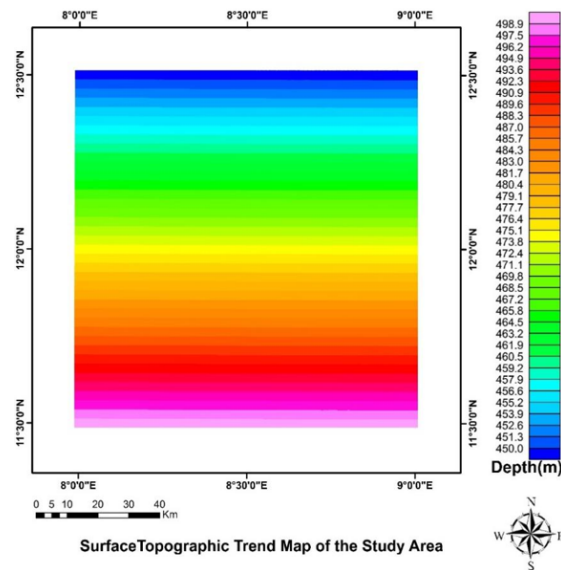


Figure 17. Regional surface topography of the study area

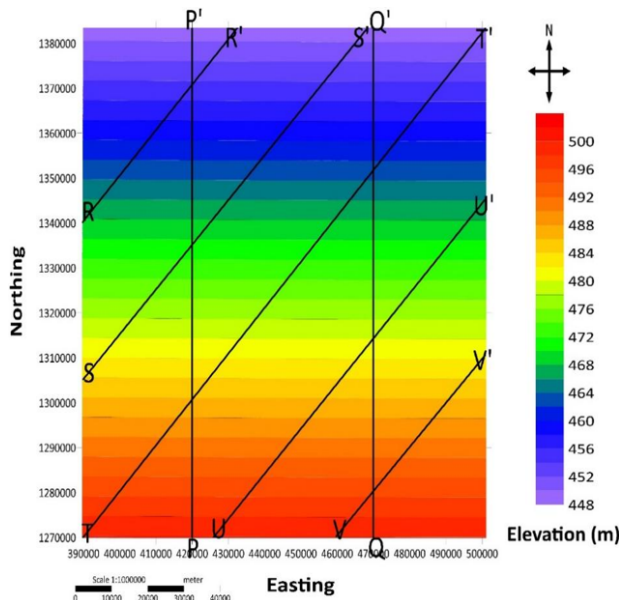


Figure 18. Regional surface topography map showing profile lines

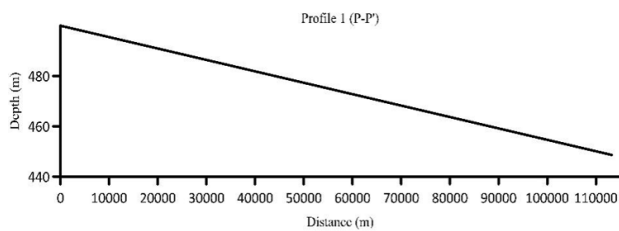


Figure 19. Profile 1 showing the cross-section P-P'

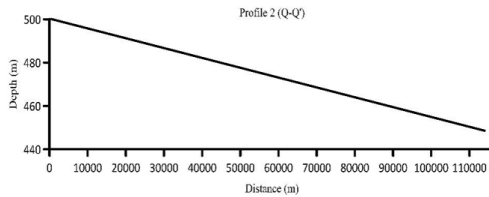


Figure 20. Profile 2 showing the cross-section Q-Q'

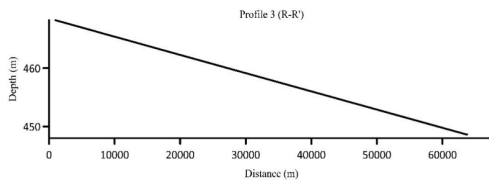


Figure 21. Profile 3 showing the cross-section R-R'

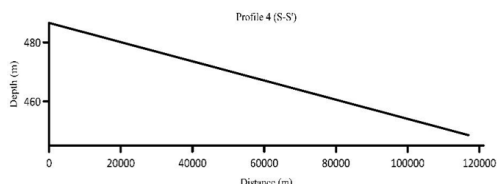


Figure 22. Profile 4 showing the cross-section S-S'

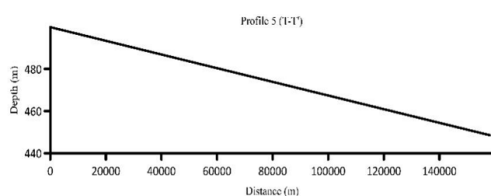


Figure 23. Profile 5 showing the cross-section T-T'

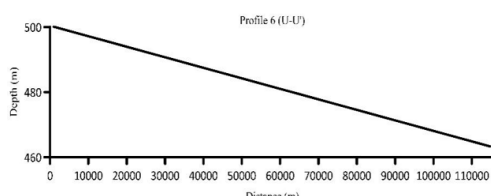


Figure 24. Profile 6 showing the cross-section U-U'

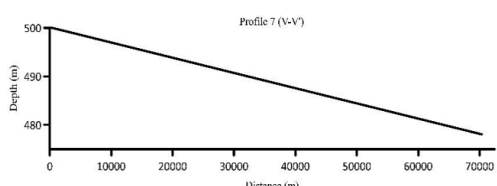


Figure 25. Profile 7 showing the cross-section V-V'

4 Interpretation of Results

Interpretation of geophysical data entails integrating information acquired from geophysical field measurements with geology, DEM and log data (such as borehole log) of the area to obtain the lithological information of the area.

4.1 Interpretation of Aeromagnetic Data

Quantitative and qualitative interpretation was adopted in this study. The qualitative interpretation of the field data was carried out by probing the TMI grid of the study area. The total magnetic field was gridded using the minimum curvature gridding. The grids generated color nuisance, and the color varied from blue to green, indicating low magnetic intensity. The yellow-to-orange color variation signifies medium magnetic. The high magnetic intensity is predominantly in the northeast to northwest, with a significant amount in the southern and southeastern parts of the study area, as shown in Figure 3. The quantitative interpretation of the TMI grids indicates varying magnetic intensity values ranging from a high intensity of 33129.4 nT to a low intensity of 32831.6 nT. The high magnetic intensity indicated by red and pink color nuisance has an intensity range of 33129.6 to 33027.4 nT; the medium magnetic intensity with color nuisance orange to yellow and lemon-green has a value range of 33023.4 to 32954.6 nT; and a low magnetic intensity with color nuisance green to blue has a value range of 32946.4 to 32831.6 nT.

4.2 Regional-Residual Separation

The RMI grid in Figure 5 shows a varying field strength ranging from 99.3 to -138.5 nT from the highest to the lowest. The highest magnetic intensity values range from 99.3 to 22.7 nT which were observed in the NE-SE and NW-SW directions of the grid. The medium RMI values were observed at the edges of the high RMI with a value range of 19.8 to -36.7 nT. The low RMI was observed in the NE-SW trend, with the SE-direction values ranging from -43.1 to -138.5 nT.

4.3 SPI

SPI was calculated using Eq. (2) from the RMI grid data to determine the depth of the magnetic source rock or basement rock of the study area. Figure 6 shows the variation in depth over the study area with a depth ranging from 25.7 m to 414.4 m. Two categories of depth were observed: the deeper depth and the shallow depth. The deeper depth values ranging from 123.2 m to 414.4 m were observed in a polygon and were marked X, Y, Z, K, M, and N. The regions marked are highly depressed zones and areas with a high tendency of groundwater accumulation. The regions of medium to shallow depth with values ranging from 25.7 m to 116.1 m were noticed around the center and southeast regions of the study area, which were marked with blue to orange color nuisance.

4.4 Topographic Trend of Basement Complex Rocks

Figure 7 shows the topographic trend of basement complex rocks in the study area. Steep slopes are in the south, southwest, and southeast regions, which gradually transition into gentler slopes towards the north, northwest, and northeast regions. The basement rocks show varying depths in topography ranging from 90 m to 118 m. The general flow path of groundwater in basement complex rocks of the study area is from the southern region to the northern region, indicating aquifers in the northern part of the study area possessing high groundwater potentiality.

4.5 DEM

Figure 16 shows the DEM map of the study area with an elevation ranging from 394 m to 566 m above the mean sea level. Higher elevations were observed in the northwest, west and southwest regions, and medium elevations were observed in the north, northeast and southeast regions of the area. Low elevations of 394 m to 421 m were observed in the northeast to northeast-east regions of the area. The map shows the drainage with a flow toward the northeast and northeast-east directions.

4.6 DEM Topographic Trend

Figure 17 shows a map of the surface topographic trend (regional DEM) in the study area. The area shows a peak region of about 490 m to 500 m in the northern region with slopes down to the southern part of the study area, indicating a depth of about 448 m to 464 m. The results show that the surface topographic trend is in the north-to-south direction, indicating that the surface flow path of fluid is in the north-to-south direction.

4.7 Profiles

Seven profiles were drawn on each of the SPI and DEM regional maps, respectively. These profiles were drawn across those maps to show the trend in the basement rock surface topography. Profiles AA', BB', PP', and QQ' were drawn perpendicular to the trend, while CC', DD', EE', FF', GG', RR', SS', TT', UU', and VV' were drawn diagonally to the trend, as shown in Figures 12 and 13.

4.7.1 Profile 1 (AA')

Figure 9 is a line drawn moving from the south to north direction in the southwest and northwest regions of the study area. This section of the area shows that the basement rock gently slopes from southwest toward the northwest direction. The profile is about 110 km long which transverses sheet 56 (Bichi) and sheet 80 (Kabo). Areas around Kunchi, Marke, Harbau, Tsanyawa, Makoda and Waire show deeper basement rock depths of about 110 to 118 m around 90 to 110 km; areas around Shakogi, Tofa, Kafin Maiko, Kadane, Doka, Goza and Kabo show medium depths of the basement rock of about 102 to 108 m around 40 to 70 km; and areas of shallow depths ranging from 90 m to 98 m are around Sayasaya, Chiromawa, Dangoro, Daurawa and Pika, which are 10 to 40 km along the profile. A tilt angle of 0.014° was observed, indicating that the basement rock topography is sloppy, meaning that groundwater flows from SW to NW direction.

4.7.2 Profile 2 (BB')

Figure 10 was drawn such that it cuts across sheets 57 and 81 running from southeast to northeast direction. The profile shows a gentle trend in topography sloping from southeast to northeast with a tilt angle of approximately 0.014°. The profile length was observed to be around 110 km long. The deeper regions were observed around 80-110 km and shallow regions around 0-20 km along the profile. Deeper areas were noticed around Marke, Ruwantsa, Gidan Dawa, Fagalama, Garin Dogo, Kore and Malamawa while shallow areas were observed around Rano, Kibiya, Sarina, Barnawa, Kafin Chiri, Garko and Darki. These indicate that there is a tendency for groundwater flow in the direction of the inferred deeper basement rock topography.

4.7.3 Profile 3 (CC')

Figure 11 indicates a profile of a length of 60 km in the northwestern part of the study area. The profile was drawn diagonally to sheet 56 around Harbau, Geza, Marke, Tsanyawa, Waire and Rage. Deeper regions of 112 to 117 m were observed around 40 to 60 km along the profile and shallow regions of 100-111 m were observed around 0 to 20 km along the profile. This indicates that the profile slopes down from the beginning to 60 km with a tilt angle of 0.010°.

4.7.4 Profile 4 (DD')

Figure 12 of a length of 110 km was drawn, cutting across sheets 80, 57 and 58. The profile passes through Kabo, Goza, Tofa, Yalwa, Kwarin Jibo and Maraki zones. Deeper regions of 110 to 117 m were observed around 80-110 km along the profile, while shallow regions of 98 to 109 km were seen from the beginning to a distance of 40 km with a tilt angle of 0.030°.

4.7.5 Profile 5 (EE')

Figure 13 shows profile 5 of a length of 156 km which cuts across sheets 80 and 57 in the southwest and northeast regions of the study area. The profile shows a shallow depth of about 90 m to 100 m around a distance of 0 to 40 km along the profile which slopes down toward a distance of about 100 km to 156 km along the profile, which is the deeper section of the profile with a depth value of about 105 m to 118 m. The profile shows an elevation angle of 0.011°, indicating that fluid flows from the shallow region to the deeper region.

4.7.6 Profile 6 (FF')

Figure 14 shows a profile of a length of 97480 m with a shallow depth of about 90 m to 100 m and a deeper depth of 100 m to 108 m with a tilt angle of 0.010°. This indicates that the profile cuts across sheets 80, 81 and 57 and slopes down toward from F to F' direction.

4.7.7 Profile 7 (GG')

Figure 15 shows profile 7 of a length of 49340 m, cutting across sheet 81. The profile shows a depth of approximately 91 m to 100 m with a tilt angle of 0.010°. This indicates that the profile is located in the shallow region of the study area.

4.7.8 Profile 1 (PP')

Figure 19 shows the profile 1 (PP') line drawn moving from south to north direction in the southwest and northwest regions of the study area. This section of the area shows that the surface topography gently slopes from northwest toward southwest direction. The profile is about 110 km long which transverses sheet 56 and sheet 80. Areas around Kunchi, Marke, Harbau, Tsanyawa, Makoda and Waire show shallow surface depths of about 480 m to 500 m around 0 to 43 km; areas around Shakogi, Tofa, Kafin Maiko, Kadane, Doka, Goza and Kabo show medium elevations between 460 m and 480 m around 43 to 89 km; and areas of deeper elevations ranging from 460 m to 440 m are around Sayasaya, Chiromawa, Dangoro, Daurawa and Pika, which are 89 to 117 km along the profile. A tilt angle of 0.025° was observed, which indicates that the surface topography is sloppy, meaning that groundwater flows from NW to SW direction.

4.7.9 Profile 2 (QQ')

Figure 20 shows profile 2 (QQ'), which was drawn such that it cuts across sheets 57 and 81 running from northeast to southeast direction. The profile shows a gentle trend in topography, sloping from northeast to southeast with a tilt angle of approximately 0.025°. The profile length was observed to be around 110 km long. The deeper regions were observed around 89-117 km and shallow regions around 0-43 km along the profile. Shallow areas were noticed around Marke, Ruwantsa, Gidan Dawa, Fagalama, Garin Dogo, Kore and Malamawa, while deeper areas were observed around Rano, Kibiya, Sarina, Barnawa, Kafin Chiri, Garko and Darki. This indicates that there is a tendency for groundwater flow in the direction of the inferred rock topography.

4.7.10 Profile 3 (RR')

Profile 3 (RR') shown in Figure 21 indicates a profile of a length of 69 km in the northwestern part of the study area. The profile was drawn diagonally to sheet 56 around Harbau, Geza, Marke, Tsanyawa, Waire and Rage. Deeper elevation regions of 455 to 448 m were observed around 43-67 km along the profile and shallow regions of 460-468 m were observed around 0-27 km along the profile. This indicates that the profile slopes down from 0 km to 69 km with a tilt angle of 0.017°.

4.7.11 Profile 4 (SS')

Profile 4 (SS') in Figure 22 shows a length of 120 km, cutting across sheets 80, 57 and 56. The profile passes through Kabo, Goza, Tofa, Yalwa, Kwarin Jibo and Maraki zones. Deeper elevation regions of 445 to 463 m were observed around 100-120 km along the profile, while shallow regions of 470-480 km were seen around 0-45 km with a tilt angle of 0.017°.

4.7.12 Profile 5 (TT')

Profile 5 (TT') in Figure 23 shows a profile of a length of approximately 160 km long, cutting across sheets 80 and 57 in the southwest and northeast regions of the study area. The profile shows a shallow elevation depth of about 480 m to 500 m around a distance of 0 to 60 km along the profile, which slopes down toward a distance of about 120 km to 160 km along the profile, which is the deeper section of the profile with a depth value of about 440 m to 460 m. The profile shows an elevation angle of 0.019°.

4.7.13 Profile 6 (UU')

Profile 6 (UU') in Figure 24 shows a profile of a length of approximately 116 km, which shows regions of a shallow elevation of about 490 to 500 m and deeper regions of 460 to 450 m with a tilt angle of 0.038°. This indicates that the profile cuts across sheets 80, 81 and 57 and slopes down toward from F to F' direction.

4.7.14 Profile 7 (VV')

Profile 7 (VV') in Figure 25 shows a profile of a length of approximately 72 km, cutting across sheet 81. The profile shows an elevation of approximately 500 to 475 m with a tilt angle of 0.017°. This indicates that the profile is located in the shallow region of the study area.

4.8 Cross Correlation

Taking the cross correlation of profiles deduced from surface and basement depths (profile 1 AA' and PP', profile 2 BB' and QQ', profile 3 CC' and RR', profile 4 DD' and SS', profile 5 EE' and TT', profile 6 FF' and UU' and profile 7 GG' and VV'), a coefficient of correlation ranging from -0.99972 to -0.9992 with an average of -0.99981 is shown in Table 3.

Table 3. Coefficient of cross correlation of the profiles

Profile	Basement Profile	Surface Profile	Correlation
1	AA'	PP'	-0.99981
2	BB'	QQ'	-0.99981
3	CC'	RR'	-0.99992
4	DD'	SS'	-0.99982
5	EE'	TT'	-0.99989
6	FF'	UU'	-0.99973
7	GG'	VV'	-0.99972
Average			-0.99981

It can be inferred that the surface and basement complex rock trends have a very poor correlation. However, the surface trend indicates accumulation at the lowest-gradient region, which could serve as the net aquifer recharge zone.

Determining regional aquifers and large-scale basin structures is the primary use of the magnetic technique in groundwater research. Because magnetic fingerprints for various sediment strata are frequently weak, and their use in mapping the unconsolidated sequence is restricted or limited. Because of the insignificant magnetic susceptibility contrast within the weathered layer and sediment, the difficulty in interpreting anomalies, and the challenges in obtaining useful quantitative information from its measurements, the method is not directly and frequently used for detailed groundwater and shallow subsurface investigation. However, information about the subsurface could be gleaned from the magnetic data thanks to a suite of reliable data processing techniques like regional-residual separation, reduce to equator, forward vertical derivative, SPI, and profile modelling that improve the characteristics of the potential field data, especially when the data quality is good and the measurement spacing is flexible.

5 Deduction

A pictographic view of TMI, RMI and SPI indicates that the area has varying magnetic anomalies with a strong magnetic intensity in the NE and NNW regions of the area and predominant low magnetic anomalies can be observed in the central and SE regions of the study area. Medium magnetic anomalies are noticed in the SWW region of the study area. It can be inferred that the basement complex rock in the area has an undulating topography with voids and peaks ranging from 25.7 m to 414.4 m. The area with a low magnetic intensity mostly consists of coarse porphyritic biotite, biotite hornblende and medium coarse-grained biotite. Areas with a high magnetic intensity mostly consist of quartz schist, biotite gneiss, sand clay and undifferentiated schist. This sudden change in rock formation and topographic discontinuity is indicative of faults, lineaments and fractures in the basement complex rock. These features are a good indication that the area could possess a high groundwater potential. The DEM map shows drainages, and high- and low-elevation zones. The regions with a low elevation are inferred as the surface water accumulation zone and could serve as aquifer recharge sources. Based on the basement complex rock topography (regional trend) in Figures 7-15, it can be inferred that the fluid flow paths are from southwest, south and southeast to northwest, north and northeast directions. The regions of groundwater accumulation are observed in the northern regions of the study area. These areas are inferred as regions with high groundwater potentials. The surface topography (surface regional trend) in Figures 17-25 shows that the general trend in the surface topography is from southwest, south and southeast to northwest, north and northeast directions, respectively. The regions of water accumulation are around the areas of low-elevation southern regions, confirming the general flow direction and may serve as aquifer net recharge sources. The regions inferred as aquifer net recharge zones may also serve as groundwater contamination sources. These contaminants could have heavy metals (Fe, Mg, Cd, Cu, Ca, etc.) from anthropogenic activities washed away by rainwater to drainages, river and water channels toward the region with a low elevation (accumulation zone).

6 Conclusion

In this study, aeromagnetic and DEM data were used to unravel the structural characteristics and the topography of the study area. Analysis of the aeromagnetic data indicates that the area has an undulating formation with varying depths ranging from 25.7 m to 414.4 m. The regional basement topography was determined to slope from the southern region to the northern region with depth values ranging from 91.0 m to 117.6 m. Analysis of the DEM data indicates a surface elevation with values ranging from 394.0 m to 565.9 m above sea level. The surface regional topography was determined to slope from the southern region to the northern region with a value range of 450.0-498.9 m. It can be summarized that the topography of both basement rock and surface is in the same direction, indicating that their water flow path is the same (S-N). It was also identified that due to the basement rock and surface topography and the flow path, groundwater and surface water accumulate in the northern region for both fresh basement complex rock and regional surface topography. It was also inferred that the contaminants washed by rainwater flow are inconsistent with the surface topography, accumulating in the accumulation zone of the surface water, which may lead to the contamination of the surface water. This accumulated water serves as the aquifer's net recharge source. It is also presumed that since the aquifer net recharge source is contaminated, the groundwater may contain large or trace amounts of contaminants. Following the fact that there is prevalent perennial agricultural activity all over the region, regulated aquifer condition monitoring is of paramount importance to forestall or prevent negative consequences resulting from stretching the aquifer capabilities. One typical example is over-salinization, which could significantly affect the flora and fauna of the ecosystem. It is recommended that frequent physicochemical analyses be carried out to investigate the water quality of the aquifer recharge sources (drainages, rivers and accumulation zones) and groundwater (hand dug wells, tube wells and boreholes) around the study area to ascertain the contamination level of groundwater. In addition, other geophysical methods like electrical resistivity imaging and the ground magnetic method can be used to determine lithology and the water bear zones in the area.

Data Availability

1. The data (aeromagnetic data) supporting our research results may be released upon application to the Nigerian Geological Survey Agency (NGSA), Abuja, Nigeria.
2. The data (DEM data) supporting our research results can be downloaded from hppts:dwtkns.com/srtm30m/

Acknowledgements

We acknowledge the effort of the Nigerian Geological Survey Agency (NGSA) and NASA for providing the data used in this research.

We are indebted to our families and colleagues for their utmost support and encouragement during the time of this research project. Their unconditional faith in our work served as a motivating force for us to succeed.

Conflicts of Interest

The authors declare that they have no conflicts of interest.

References

- [1] A. Usman, M. Sani, K. Lawal, and S. Magaji, “Aeromagnetic investigation of geologic structures associated with gold mineralization along danja, northwestern Nigeria,” *Bima J. Sci. Technol.*, vol. 3, no. 1, pp. 184–195, 2019.
- [2] C. Ndikilar, B. Idi, B. Terhemba, I. Idowu, and S. Abdullahi, “Applications of aeromagnetic and electrical resistivity data for mapping spatial distribution of groundwater potentials of Dutse, Jigawa State, Nigeria,” *Mod. Appl. Sci.*, vol. 13, no. 2, pp. 11–20, 2019. <https://doi.org/10.5539/mas.v13n2p11>
- [3] D. Abdullahi and J. Ejepu, “Aeromagnetic and resistivity surveying for delineating optimal sites for groundwater development in part of Minna, Sheet 164 SW, North-Central Nigeria,” *Minna J. Geosci.*, 2018.
- [4] A. Kouame, M. Ta, B. Akokponhoue, O. De Lasme, and L. Kouam'e, “Contribution of aeromagnetic data to the structural discontinuities identification of black volta catchment aquifer system in côte d'ivoire,” *ESI Prepr.*, vol. 19, no. 30, p. 307, 2023. <https://doi.org/10.19044/esj.2023.v19n30p307>
- [5] O. Ademila, “Integrated geophysical methods for subsurface characterisation and health hazard assessment in parts of southwestern basement Nigeria,” *IOP Conf. Ser. Earth Environ. Sci.*, vol. 173, no. 1, p. 012024, 2018. <https://doi.org/10.1088/1755-1315/173/1/012024>
- [6] C. Okpoli and B. Akinbulejo, “Aeromagnetic and electrical resistivity mapping for groundwater development around ilesa schist belt, southwestern Nigeria,” *J. Pet. Explor. Prod. Technol.*, vol. 12, pp. 555–575, 2021. <https://doi.org/10.1007/s13202-021-01307-x>
- [7] E. O. Wasiu, O. O. Wasiu, I. T. Abel, A. F. Fagbemigun, and T. S. Fagbemigun, “Aeromagnetic interpretation of basement structures and geometry in parts of the middle Benue trough, North Central, Nigeria,” *Adv. Geol. Geotech. Eng. Res.*, vol. 4, no. 4, pp. 22–40, 2022. <https://doi.org/10.30564/agger.v4i4.5128>
- [8] I. S. Olubusola, A. Isaac, O. K. Oyamenda, and B. M. Adesola, “Assessment of groundwater occurrence in a typical schist belt region in Osun State, Southwestern Nigeria using VES, aeromagnetic dataset, remotely sensed data, and MCDA approaches,” *Sustain. Water Resour. Manag.*, vol. 9, no. 1, p. 29, 2023. <https://doi.org/10.1007/s40899-022-00810-1>
- [9] N. B. Salawu, “Aeromagnetic and digital elevation model constraints on the structural framework of southern margin of the Middle Niger Basin, Nigeria,” *Sci. Rep.*, vol. 11, no. 1, p. 21646, 2021. <https://doi.org/10.1038/s41598-021-00829-y>
- [10] H. T. El-Badrawy, A. M. Abbas, U. Massoud, T. Abu-Alam, H. A. Alrefae, S. M. Abo Khashaba, and M. Nagy, “Integrated approach-based groundwater mapping in sohag governorate, upper Egypt, using remote sensing and aeromagnetic data,” *Front. Earth Sci.*, vol. 12, p. 1456055, 2024. <https://doi.org/10.3389/feart.2024.1456055>
- [11] M. Mokarram, M. Shaygan, and D. Sathyamoorthy, “Using DEM and GIS for evaluation of groundwater resources in relation to landforms in the Maharlou-Bakhtegan watershed, Fars province, Iran,” *J. Water Land Dev.*, vol. 37, no. 1, pp. 121–126, 2018. <https://doi.org/10.2478/jwld-2018-0031>
- [12] A. Ibrahim, T. S. Y. Thoong, M. A. Mohammed, N. M. Nasidi, M. D. Zakari, and M. M. Maina, “Mapping groundwater vulnerability to potential contamination in Kano metropolis - Nigeria,” *Techno Sci. Afr. J.*, vol. 14, no. 1, pp. 181–194, 2017.
- [13] W. Lowrie, *Fundamentals of Geophysics*. Cambridge University Press, 2007.
- [14] W. M. Telford, L. P. Geldart, and R. E. Sheriff, *Applied Geophysics*. Cambridge University Press, 1990.
- [15] O. C. Ezech, G. Egwuonwu, C. Amadansun, and M. Umego, “Source parameter imaging of aeromagnetic map of Sokoto Basin, Northwestern Nigeria,” *Int. J. Mech. Civ. Eng.*, vol. 4, no. 1, pp. 1–11, 2021.
- [16] N. G. Obaje, *Geology and Mineral Resources of Nigeria*. Springer, 2009.

- [17] M. B. Yakubu, K. M. Lawal, B. B. M. Dewu, and A. E. Ikpokonte, "Investigation of geothermal energy resource potential using aero-magnetic and aero-radiometric data of Kano, Nigeria," *Fudma J. Sci.*, vol. 6, no. 1, pp. 296–307, 2022. <https://doi.org/10.33003/fjs-2022-0601-900>
- [18] A. G. Tahir, I. Garba, and M. B. Girie, "Subsurface lithology and aquifer zones using vertical electrical sounding method in Kano Metropolis, Northwestern Nigeria," *IOSR J. Appl. Geol. Geophys.*, vol. 2, no. 6, pp. 46–51, 2014.
- [19] A. H. Suleiman, "Pattern of water supply in relation to different water sources in metropolitan Kano," *Fudma J. Sci.*, vol. 4, no. 3, pp. 690–696, 2020. <https://doi.org/10.33003/fjs-2020-0403-432>
- [20] A. E. Bala, O. M. Eduvie, and J. Byami, "Borehole depth and regolith aquifer hydraulic characteristics of bedrock types in Kano area, Northern Nigeria," *Afr. J. Environ. Sci. Technol.*, vol. 5, no. 3, pp. 228–237, 2011. <https://doi.org/10.5897/AJEST10.194>
- [21] A. M. MacDonald and J. Davies, "A brief review of groundwater for rural water supply in sub-Saharan Africa," Technical Report WC/00/33, 2000.
- [22] T. Y. Rilwanu, "Electrical resistivity survey for groundwater exploration in the basement terrain of Kano State, Nigeria," *Gashua J. Sci. Humanit.*, vol. 2, no. 2, pp. 137–146, 2016.